International Journal of Solids and Structures 56–57 (2015) 20–28

Contents lists available at ScienceDirect

International Journal of Solids and Structures

journal homepage: www.elsevier.com/locate/ijsolstr

Temperature-responsive bending of a bilayer gel

Takuya Morimoto *, Fumihiro Ashida

Interdisciplinary Graduate School of Science and Engineering, Shimane University, 1060 Nishikawatsu, Matsue, Shimane 690-8504, Japan

ARTICLE INFO

Article history:
Received 16 September 2014
Received in revised form 28 November 2014
Available online 17 December 2014

Keywords:
Finite bending
Gels
Bilayers
Swelling
Actuation

ABSTRACT

We investigate the finite bending of a bilayer gel in response to temperature under plane strain condition. We demonstrate that our model based on finite elasticity predicts larger bending curvatures of the bilayers compared with the linear model based on the elementary beam theory, and a high swelling ratio in the bilayer enhances the differences between both models. We also show that the folding shape of the bilayer can be controlled by tuning the ratio of shear modulus and the length-to-height ratio and that multiple neutral axes can exist in the bilayer under certain conditions. Our results could provide the basis for further numerical modeling of a layered gel as well as a spatially patterned gel to create 3D complex self-folding structures.

1. Introduction

Soft materials that undergo a desired three-dimensional (3D) shape transformation in response to changes in ambient environment have potential applications in soft robotics (Osada and Gong, 1998; Calvert, 2009; Hawkes et al., 2010; Majidi, 2014), biomedicine (Peppas et al., 2006; Hoare and Kohane, 2008; Annabi et al., 2013), biomedical devices (Bashir, 2004; Azam et al., 2010; Randall et al., 2012), optical devices (Dong et al., 2006), microfluidic devices (Richter et al., 2004; Jamal et al., 2011), and responsive surfaces (Stuart et al., 2010). The large reversible deformation of soft materials in response to a specific external stimulus such as temperature (Hu et al., 1995; Asoh et al., 2008; Zhang et al., 2012; Kim et al., 2012; Kim et al., 2012), solvent (Guan et al., 2005; Kelby et al., 2011; Jeong et al., 2011; Holmes et al., 2011), pH (Luchnikov et al., 2005; Kumar et al., 2009; Kelby et al., 2011), light (Jamal et al., 2011; Yu et al., 2003), and electric field (Smela et al., 1995; Fukunaga et al., 2008) can be utilized to create a self-folding/self-shaping structure which broadly refers to a class of self-assembly systems in which the structures curve or fold-up either spontaneously (Gracias, 2013; Ionov, 2014; Studart and Erb, 2014).

In particular, temperature-responsive hydrogels can exhibit extremely large deformation due to the volume transition in response to changes in temperature (Hu et al., 1995; Asoh et al., 2008; Zhang et al., 2012; Kim et al., 2012; Kim et al., 2012). A prime example is based on poly(*N*-isopropylacrylamide) (PNIPA), which has a lower critical solution temperature (LCST) around room temperature, 305 K. PNIPA-based temperature-responsive gels dramatically increase their volume by as much as a factor of 10 when the temperature decreases from above the LCST to below it. The PNIPA gels have been studied extensively, and a large number of experiments are available (Schild, 1992). In order to design structures that fold in response to temperature, one of the strategies is to generate spatially inhomogeneous differential stresses either along its thickness or lateral directions so that a bending moment is generated. A straightforward strategy to create a temperature-responsive bending structure is to utilize a layered structure. Hu et al. (1995) have first fabricated partially interpenetrated polymer networks composed of PNIPA and poly(acrylamide) (PAAM), so-called "bi-gels" which bend into circles in response to variations in acetone concentration or temperature. They demonstrated that a hand-like device gripped the object at 308 K and released it at room temperature, 295 K. Bending is achieved when one of the polymer layers swells more than the other, by a response to temperature. This strategy harnessing inhomogeneous swelling through the thickness creates one-dimensional structures that can bend into a shape with mean curvature (Hu et al., 1995; Asoh et al., 2008; Zhang et al., 2012; Agrawal et al., 2014; Topham et al., 2007; Swann and Ryan, 2009; Smela et al., 1995).

The design principle of bending actuation using a layered structure is not new and dates back to a bimetal strip. The British clockmaker John Harrison has innovated the bimetal strip thermometer in a seventeenth century, and then Timoshenko (1925) has first achieved the analysis of the thermoelastic deformation in bimetal strips as functions of the geometry and mismatch in material properties. The curvature of the bimetal strip, where the thickness of each layer is same, is proportional to the difference in elongation

* Corresponding author.
E-mail address: morimoto@riko.shimane-u.ac.jp (T. Morimoto).

http://dx.doi.org/10.1016/j.ijsolstr.2014.12.009
0020-7683/

of the two layers and inversely proportional to the thickness of the bilayer without external forces. Since hydrogels can cause significantly larger volume changes due to swelling, compared with the actuation by thermal expansion in metals, the bilayer gel can actuate with extremely large deformation and realize the creation of self-folding structures. Recently, Lucantonio et al. (2014) have described swelling-induced bending of bilayered gel beams. They have also proposed two simple formulae for the axial stretching and bending curvature, depending on the material and geometrical parameters such as the shear modulus ratio and the thickness ratio. Chester et al. (2015) have implemented the theory of Chester and Anand (2011) for fluid diffusion and large deformations of elastomeric gels in the commercial finite-element code Abaqus/Standard. As one of illustrative examples to demonstrate the robustness of the numerical implementation, they have performed a finite element simulation of a thermally responsive bilayer within the framework of a thermo-chemo-mechanically coupled theory.

More complex 3D shape transformation of patterned gels has been achieved by an alternative approach using an in-plane inhomogeneous swelling that is based on the concept coined as "non-Euclidean target metric" (Klein et al., 2007; Sharon and Efrati, 2010; Kim et al., 2012; Byun et al., 2013; Therien-Aubin et al., 2013; Wu et al., 2013). The in-plane variations in swelling induce out-of-plane buckling into a 3D shape with both mean and Gaussian curvature. However, at present, the understanding of how patterned gels transform into 3D complex shapes remains far from understood. Therefore, a detailed analytical study of bilayer gel which is the simplest and most commonly employed geometry with mean curvature promises to help understanding for more complex 3D shape transformation of patterned gels.

Here, we investigate the finite bending of a bilayer gel in response to temperature under plane strain condition. We first decompose the deformation gradient into the one-dimensional homogeneous swelling part and the non-swelling homogeneous pure bending part. Then, we impose the self-equilibrium condition that the bending moment through the bilayer gel is mechanically balanced without any external forces and numerically determine the equilibrium shapes. We demonstrate that our analysis based on finite elasticity predicts larger curvatures of the bilayers compared with the linear model based on the elementary beam theory. Finally, we further examine the influences of the length-to-height ratio of bilayer and the ratio of shear modulus between two layers on the shapes and stress distributions. We show that the folding shape of the bilayer can be controlled by tuning the ratio of shear modulus and the length-to-height ratio and that multiple neutral axes can exist in the bilayer under certain conditions.

2. Finite bending of a bilayer gel in plane strain condition

In Fig. 1, we schematically show a problem setting for finite bending of a bilayer gel in response to temperature T. A bilayer gel is stacked with two layers of temperature-responsive gel having different swelling ratios, as shown in Fig. 1(A). When the bilayer gel is immersed in solution with temperature T, each gel layer can be bent due to swelling without any external forces according to the relative value of the swelling ratios between two gels. In order to illustrate finite bending of a bilayer gel due to swelling in the simplest settings, we shall consider specific bilayer gel consisting of an incompressible elastomer (non-swellable gel) layer ($s=1$) and a gel layer ($s=2$), as shown in Fig. 1(B). This bilayer gel is equivalent to that consisting of two gel layers if the swelling ratio of the gel layer is regarded as the relative one instead of those of two gel layers.

In order to describe the equilibrium for finite bending and swelling phenomena of the hydrogel, we specify the Helmholtz free energy density. The free energy density function of the (s)th layer per unit *dry* volume $V_0^{(s)}$ is described by the Flory–Rehner model (Flory and Rehner, 1943) in terms of principal stretches $\lambda_i^{(s)}$ $(i=1,2,3)$, which consists of two terms:

$$W^{(s)} = W_{\mathrm{e}}^{(s)}\left(\lambda_1^{(s)},\lambda_2^{(s)},\lambda_3^{(s)};T\right) + J^{(s)}W_{\mathrm{m}}^{(s)}\left(\phi^{(s)};T\right), \tag{1}$$

where the volume ratio $J^{(s)}=\lambda_1^{(s)}\lambda_2^{(s)}\lambda_3^{(s)}=V^{(s)}/V_0^{(s)}$ is the scale factor to represent it in the *dry* state since $\phi^{(s)}$ is the volume fraction of polymer in the *current* state. The first term is the free energy density associated with the elastic deformation of the polymer network. The Gaussian chain network model with the compressibility gives

$$W_{\mathrm{e}}^{(s)}\left(\lambda_1^{(s)},\lambda_2^{(s)},\lambda_3^{(s)};T\right)=\frac{G^{(s)}}{2}\left[\left(\lambda_1^{(s)}\right)^2+\left(\lambda_2^{(s)}\right)^2+\left(\lambda_3^{(s)}\right)^2-3-2\ln J^{(s)}\right], \tag{2}$$

in which the last term on right hand side represents contributions to the entropy change due to volume changes: the compressibility. For elastomer layer ($s=1$), we set $J^{(1)}=1$ to yield the incompressible neo-Hooke model, $W_{\mathrm{e}}^{(1)}$. $G^{(s)}=n^{(s)}k_{\mathrm{B}}T$ is the shear modulus of elasticity in the dry state, $n^{(s)}$ is the crosslink density, T is temperature, and $k_{\mathrm{B}}=1.38\times10^{-23}$ J/K is Boltzmann's constant. The second term in Eq. (1) is the mixing free energy due to the mixing of the polymer network and the solvent. A simple model for the mixing term is taken to be the mixing energy for a polymer solution of the form (Doi, 2009):

$$W_{\mathrm{m}}^{(s)}\left(\phi^{(s)};T\right)=\frac{k_{\mathrm{B}}T}{v_{\mathrm{s}}}\left[\left(1-\phi^{(s)}\right)\ln\left(1-\phi^{(s)}\right)+\chi^{(s)}\left(\phi^{(s)};T\right)\phi^{(s)}\left(1-\phi^{(s)}\right)\right], \tag{3}$$

where v_{s} is the volume per solvent molecule; $\phi^{(s)}$ is the volume fraction of polymer in swollen state and that of dry state is set to unity. Based on the assumption that the polymer network and pure liquid solvent are incompressible, the volume fraction of polymer, $\phi^{(s)}$, is related to the nominal concentration of solvent, C, by Hong et al. (2008) and Chester and Anand (2010)[1]

$$1+v_{\mathrm{s}}C=1/\phi^{(s)}=J^{(s)}. \tag{4}$$

The dimensionless parameter $\chi^{(s)}(\phi^{(s)};T)$ is a function of the volume fraction of polymer and temperature, which is experimentally measured in the following form (Afroze et al., 2000; Cai and Suo, 2011):

$$\chi^{(s)}(\phi^{(s)};T)=\chi_0+\chi_1\phi^{(s)}, \tag{5}$$

where $\chi_0=A_0+B_0T$ and $\chi_1=A_1+B_1T$. Eq. (5) represents the disaffinity between the polymer and solvent. Therefore, the free energy density describing the equilibrium of the gel may be represented as a function of temperature through the $\chi^{(s)}$-parameter. A Legendre transform allows us the free energy density function $W^{(s)}$ to be transformed into another form $\tilde{W}^{(s)}$ as a function of chemical potential μ instead of $\phi^{(s)}$ (Hong et al., 2008),

$$\tilde{W}^{(s)}\left(\lambda_1^{(s)},\lambda_2^{(s)},\lambda_3^{(s)},\mu;T\right)=W^{(s)}\left(\lambda_1^{(s)},\lambda_2^{(s)},\lambda_3^{(s)},\phi^{(s)};T\right)-\frac{\mu}{v_{\mathrm{s}}}\left(J^{(s)}-1\right). \tag{6}$$

The equations of state that describe the mechano-chemical interaction of the hydrogels give the principal true stresses (Cai and Suo, 2011),

$$\sigma_i^{(s)}=\frac{\lambda_i^{(s)}}{J^{(s)}}\frac{\partial\tilde{W}}{\partial\lambda_i^{(s)}},\quad (i=1,2,3). \tag{7}$$

[1] Here we can find an alternative formulation of swelling-induced large deformations in polymer gels (Lucantonio et al., 2013) where the nominal concentration of solvent C is defined as a state variable at the starting point.

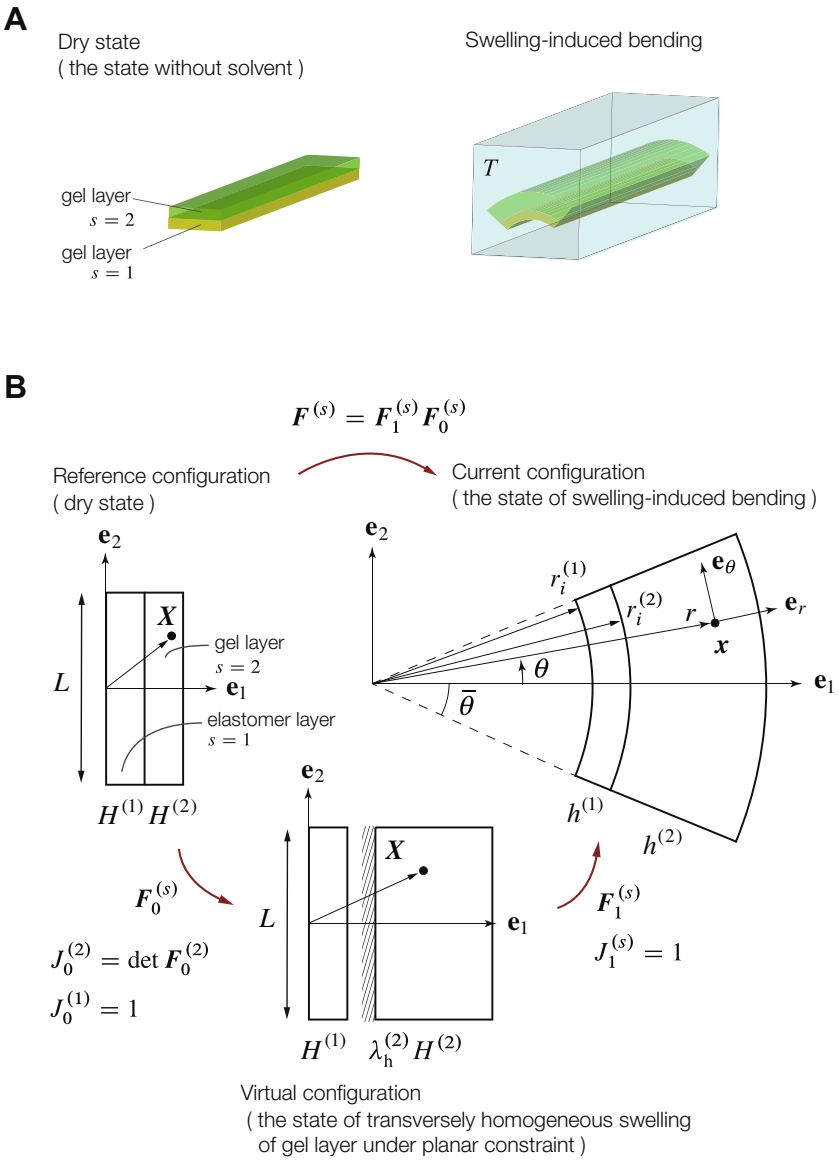

Fig. 1. Problem setting. (A) Swelling-induced bending of a bilayer gel from dry state due to the difference of swelling ratios. (B) Coordinate systems and schematic of the multiplicative decomposition.

We decompose the deformation gradient, $\mathbf{F}^{(s)}$, from the dry state to the state of swelling-induced bending into two parts as shown in Fig. 1(B): $\mathbf{F}^{(s)} = \mathbf{F}_1^{(s)}\mathbf{F}_0^{(s)}$ where $\mathbf{F}_0^{(s)}$ is for the kinematics from the dry state (reference configuration) to the state of one-dimensional swelling under plane constraint (intermediate configuration), and $\mathbf{F}_1^{(s)}$ is for the kinematics from the virtual configuration to the swelling-induced bending state (current configuration). When the constraint is released, the bilayer gel is bent due to the unbalanced stresses. This multiplicative decomposition for swelling gels has been adapted widely in the literature (Duda et al., 2010; Chester and Anand, 2010; Lucantonio et al., 2013), and in the present study it is useful to capture the role that the swelling under constraint builds up compressive stress in the strip.

We first consider the one-dimensional swelling of the gel (Kang and Huang, 2010) from the dry state whereas the elastomer is still in deformation-free, $\mathbf{F}_0^{(1)} = \mathbf{I}$ where $\mathbf{I}$ is the identity tensor. We assume that the gel layer can only stretch in the thickness direction ($\mathbf{e}_1$-direction) due to swelling in response to temperature. As a result, biaxial compressive stresses build up in the gel layer. In this kinematics, the deformation gradient of the gel layer can be expressed as

$$\mathbf{F}_0^{(2)} = \lambda_1^{(2)}\mathbf{e}_1 \otimes \mathbf{e}_1 + \lambda_2^{(2)}\mathbf{e}_2 \otimes \mathbf{e}_2 + \lambda_3^{(2)}\mathbf{e}_3 \otimes \mathbf{e}_3, \tag{8}$$

where

$$\lambda_1^{(2)} = \lambda_{\mathrm{h}}^{(2)}, \quad \lambda_2^{(2)} = \lambda_3^{(2)} = 1. \tag{9}$$

Substituting Eqs. (1) and (9) into Eq. (7), we have the equi-biaxial stresses in the $\mathbf{e}_2\mathbf{e}_3$-plane, $\sigma_0^{(2)} \equiv \sigma_2^{(2)} = \sigma_3^{(2)}$, and the stress in the transverse direction $\mathbf{e}_1$, $\sigma_1^{(2)}$:

$$\frac{\sigma_0^{(2)} v_{\mathrm{s}}}{k_{\mathrm{B}}T} = \ln\left(1 - \frac{1}{\lambda_{\mathrm{h}}^{(2)}}\right) + \frac{1}{\lambda_{\mathrm{h}}^{(2)}} + \left(\frac{\chi_0 - \chi_1}{\left(\lambda_{\mathrm{h}}^{(2)}\right)^2} + \frac{2\chi_1}{\left(\lambda_{\mathrm{h}}^{(2)}\right)^3}\right) - \frac{\mu}{k_{\mathrm{B}}T}, \tag{10}$$

$$\frac{\sigma_1^{(2)} v_{\mathrm{s}}}{k_{\mathrm{B}}T} = \frac{n^{(2)} v_{\mathrm{s}}}{\lambda_{\mathrm{h}}^{(2)}}\left(\left(\lambda_{\mathrm{h}}^{(2)}\right)^2 - 1\right) + \ln\left(1 - \frac{1}{\lambda_{\mathrm{h}}^{(2)}}\right) + \frac{1}{\lambda_{\mathrm{h}}^{(2)}} + \left(\frac{\chi_0 - \chi_1}{\left(\lambda_{\mathrm{h}}^{(2)}\right)^2} + \frac{2\chi_1}{\left(\lambda_{\mathrm{h}}^{(2)}\right)^3} - \frac{\mu}{k_{\mathrm{B}}T}\right). \tag{11}$$

The external chemical potential of the outer solvent is given by $\hat{\mu} = \mu_0 + v_{\mathrm{s}}\hat{p}$, where μ_0 is a reference chemical potential and $\hat{p}$ is

the external pressure. We set $\mu_0 = 0$ for simplicity through this paper. In equilibrium with an incompressible liquid solvent, we have $\mu = \hat{\mu} = 0$ and the corresponding external pressure $\hat{p}$ is taken to be zero. Thus, the top surface of gel layer can be assumed to be traction-free: $\sigma_1^{(2)} = -\hat{p} = 0$. Solving Eq. (11) under these boundary conditions, the equilibrium swelling ratio of the gel which is equivalent to the stretch in the thickness direction, $\lambda_{\mathrm{h}}^{(2)}$, can be determined by

$$\frac{n^{(2)}v_{\mathrm{s}}}{\lambda_{\mathrm{h}}}(\lambda_{\mathrm{h}}^2-1)+\ln\left(1-\frac{1}{\lambda_{\mathrm{h}}}\right)+\frac{1}{\lambda_{\mathrm{h}}}\left(\frac{\chi_0-\chi_1}{\lambda_{\mathrm{h}}^2}+\frac{2\chi_1}{\lambda_{\mathrm{h}}^3}\right)=0. \tag{12}$$

This is a compressive biaxial stress induced by swelling of the confined gel due to a layered structure.

Next, we consider the kinematics of bilayer gel from the state of the one-dimensional swelling to the state of finite pure bending. This kinematics can be considered as a pure bending of layered elastomer with no volume change. This problem has already been solved when we assume that the homogeneous finite deformation to each layer regarding as a plane strain problem. As shown in Fig. 1(B), the position vectors in the virtual configuration and the current configuration are denoted by $\mathbf{X} = (X_1, X_2, X_3)$ and $\mathbf{x} = (r, \theta, z)$, respectively. The deformation gradient for both layers ($s = 1, 2$) is given by (Rivlin, 1949; Roccabianca et al., 2010):

$$\mathbf{F}_1^{(s)} = \frac{L}{2\bar{\theta}r}\mathbf{e}_r \otimes \mathbf{e}_1 + \frac{2\bar{\theta}r}{L}\mathbf{e}_\theta \otimes \mathbf{e}_2 + \mathbf{e}_z \otimes \mathbf{e}_3. \tag{13}$$

The volume conservation from the one-dimensional swollen state to the pure bending imposes

$$2\bar{\theta}h^{(s)}\left(r_i^{(s)}+\frac{h^{(s)}}{2}\right) = LH^{(s)}\lambda_{\mathrm{h}}^{(s)}, \tag{14}$$

where $\lambda_{\mathrm{h}}^{(1)} = 1$ for an incompressible elastomer and $\lambda_{\mathrm{h}}^{(2)} \neq 1$ is determined by Eq. (12) for gel layer. From Eq. (14), we have $r_i^{(s+1)} = r_i^{(s)} + h^{(s)}$ where $r_i^{(1)} = \frac{LH^{(1)}}{2\bar{\theta}h^{(1)}}\lambda_{\mathrm{h}}^{(1)} - \frac{h^{(1)}}{2}$. Thus, Eq. (14) also gives the thickness of gel layer ($s = 2$),

$$h^{(2)} = -\frac{LH^{(1)}}{2\bar{\theta}h^{(1)}} - \frac{h^{(1)}}{2} + \sqrt{\left(\frac{LH^{(1)}}{2\bar{\theta}h^{(1)}}+\frac{h^{(1)}}{2}\right)^2 + \frac{LH^{(2)}}{\bar{\theta}}\lambda_{\mathrm{h}}^{(2)}}. \tag{15}$$

Finally, we consider the kinematics from the dry state to the swelling-induced bending state. As shown in Fig. 1(B), in the dry state, we assume the layers to be stress-free state and introduce a Cartesian coordinate system. In the current configuration, we assume that each layer is isochoricly deformed as a sector of a cylindrical tube of semi-angle $\bar{\theta}$ and introduce a cylindrical coordinate system (r, θ, z). The deformation gradients from the dry state to the swelling-induced bending state is obtained by multiplying the deformation gradients

$$\mathbf{F}^{(s)} = \mathbf{F}_1^{(s)}\mathbf{F}_0^{(s)} = \frac{L}{2\bar{\theta}r}\lambda_{\mathrm{h}}^{(s)}\mathbf{e}_r \otimes \mathbf{e}_1 + \frac{2\bar{\theta}r}{L}\mathbf{e}_\theta \otimes \mathbf{e}_2 + \mathbf{e}_z \otimes \mathbf{e}_3, \tag{16}$$

so that we have the stretches, $\lambda_r^{(s)} = \frac{L}{2\bar{\theta}r}\lambda_{\mathrm{h}}^{(s)}$, $\lambda_\theta^{(s)} = \frac{2\bar{\theta}r}{L}$, and $\lambda_z^{(s)} = 1$. The balance equations of the sth layer are

$$\frac{\partial\sigma_r^{(s)}}{\partial r}+\frac{\sigma_r^{(s)}-\sigma_\theta^{(s)}}{r}=0, \quad \frac{\partial\sigma_\theta^{(s)}}{\partial\theta}=0. \tag{17}$$

Since the stretches depend only on r, the chain rule of differentiation of the free energy function can be expressed as $\frac{\mathrm{d}\bar{W}^{(s)}}{\mathrm{d}r} = \frac{\mathrm{d}\sigma_r^{(s)}}{\mathrm{d}r}\lambda_{\mathrm{h}}^{(s)}$. In addition, $\sigma_\theta^{(s)}$ only depends on r, the stress in radial direction yields

$$\sigma_r^{(s)} = \bar{W}^{(s)}\left(\lambda_\theta^{(s)}(r)\right) + \gamma^{(s)}, \tag{18}$$

where we have redefined $\bar{W}^{(s)}$ at $\hat{\mu} = 0$ in Eq. (6) as

$$\bar{W}^{(s)}\left(\lambda_\theta^{(s)}(r)\right) = \frac{1}{\lambda_{\mathrm{h}}^{(s)}}\tilde{W}^{(s)}\left(\frac{\lambda_{\mathrm{h}}^{(s)}}{\lambda_\theta^{(s)}(r)}, \lambda_\theta^{(s)}(r), 1, 0; T\right). \tag{19}$$

Substitution Eq. (19) into $(17)_1$ gives the stress in hoop direction,

$$\sigma_\theta^{(s)} = r\frac{\partial\sigma_r}{\partial\lambda_\theta^{(s)}}\frac{\partial\lambda_\theta}{\partial r} + \sigma_r^{(s)} = \lambda_\theta^{(s)}\frac{\partial\bar{W}^{(s)}}{\partial\lambda_\theta^{(s)}} + \bar{W}^{(s)}\left(\lambda_\theta^{(s)}(r)\right) + \gamma^{(s)}, \tag{20}$$

where $\gamma^{(s)}$ is an unknown integration constant, which is determined by imposing the continuity condition of traction at interfaces between layers and traction-free boundary conditions at the external boundaries of the bilayer gel:

$$\left.\begin{aligned} &\sigma_r^{(1)}\left(r_i^{(1)}+h^{(1)}\right) = \sigma_r^{(2)}\left(r_r^{(2)}\right), \\ &\sigma_r^{(1)}\left(r_i^{(1)}\right) = 0, \quad \sigma_r^{(2)}\left(r_i^{(2)}+h^{(2)}\right) = 0. \end{aligned}\right\} \tag{21}$$

Substituting Eqs. (18) and (20) into Eq. (21), the unknown integration constants are obtained as

$$\gamma^{(1)} = -\bar{W}^{(1)}\left(\lambda_\theta^{(1)}\left(r_i^{(1)}\right)\right), \quad \gamma^{(2)} = -\bar{W}^{(2)}\left(\lambda_\theta^{(2)}\left(r_i^{(2)}+h^{(2)}\right)\right). \tag{22}$$

No external forces are applied to the bilayer gel in the swollen state. The resultant force balance requires that

$$\int_0^{h^{(1)}}\sigma_\theta^{(1)}\,\mathrm{d}r + \int_{h^{(1)}}^{h^{(2)}}\sigma_\theta^{(2)}\,\mathrm{d}r = 0, \tag{23}$$

$$\int_0^{h^{(1)}}\sigma_\theta^{(1)}r\,\mathrm{d}r + \int_{h^{(1)}}^{h^{(2)}}\sigma_\theta^{(2)}r\,\mathrm{d}r = 0. \tag{24}$$

The total thickness of bilayer gel in the current configuration is given by $h = h^{(1)} + h^{(2)}$. Since we assumed that the surface of the gel is traction-free, Eq. (23) is automatically satisfied. Thus, we only require Eq. (24) to be satisfied and numerically solve for the unknown kinematic parameters $(\bar{\theta}, h^{(1)})$ to determine the self-equilibrium state.

The closed form expressions of stress components can be derived by Eqs. (18) and (20) with Eqs. (19) and (22):

$$\left.\begin{aligned} \sigma_r^{(1)} &= \tfrac{G^{(1)}}{2}\left[\tfrac{L^2}{4\bar{\theta}^2}\left(\tfrac{1}{r^2}-\tfrac{1}{\left(r_i^{(1)}\right)^2}\right)+\tfrac{4\bar{\theta}^2}{L^2}\left((r^2)-\left(r_i^{(1)}\right)^2\right)\right], \\ \sigma_\theta^{(1)} &= \tfrac{G^{(1)}}{2}\left[\tfrac{4\bar{\theta}^2}{L^2}\left(3r^2-\left(r_i^{(1)}\right)^2\right)-\tfrac{L^2}{4\bar{\theta}^2}\left(\tfrac{1}{r^2}+\tfrac{1}{\left(r_i^{(1)}\right)^2}\right)\right], \end{aligned}\right\} \tag{25}$$

with $r_i^{(1)} = \frac{LH^{(1)}}{2\bar{\theta}h^{(1)}}\lambda_{\mathrm{h}}^{(1)} - \frac{h^{(1)}}{2}$ for the elastomer layer, and

$$\left.\begin{aligned} \sigma_r^{(2)} &= \tfrac{G^{(2)}}{2}\left[\tfrac{L^2}{4\bar{\theta}^2\lambda_{\mathrm{h}}}\left(\tfrac{1}{r^2}-\tfrac{1}{\left(r_i^{(3)}\right)^2}\right)+\tfrac{4\bar{\theta}^2\lambda_{\mathrm{h}}}{L^2}\left((r^2)-\left(r_i^{(3)}\right)^2\right)\right], \\ \sigma_\theta^{(2)} &= \tfrac{G^{(2)}}{2}\left[\tfrac{4\bar{\theta}^2}{L^2\lambda_{\mathrm{h}}}\left(3r^2-\left(r_i^{(3)}\right)^2\right)-\tfrac{L^2\lambda_{\mathrm{h}}}{4\bar{\theta}^2}\left(\tfrac{1}{r^2}+\tfrac{1}{\left(r_i^{(3)}\right)^2}\right)\right], \end{aligned}\right\} \tag{26}$$

with $r_i^{(3)} = r_i^{(2)} + h^{(2)}$ and $r_i^{(2)} = r_i^{(1)} + h^{(1)}$ for the gel layer.

3. Results and discussion

The free energy density function given by Eq. (1) or (19) introduces five parameters: a dimensionless measure of the crosslink density, $n^{(2)}v_{\mathrm{s}}$, and the four fitting parameters to the specific PNIPA-based gel, (A_0, B_0, A_1, B_1), which are provided by (Afroze et al., 2000; Cai and Suo, 2011) as

$$A_0 = -12.947, \quad B_0 = 0.04496\ \mathrm{K}^{-1},$$
$$A_1 = 17.92, \quad B_1 = -0.0569\ \mathrm{K}^{-1}.$$

The volume per solvent (water) molecule is usually given as $v_{\mathrm{s}} = 3\times10^{-29}\ \mathrm{m}^3$. In addition, as a simple setting, we specifically

choose $H^{(1)} = H^{(2)}$ for the initial thickness of each layer and $G^{(1)} = 1$ MPa for the shear modulus of elastomer layer at $T = 300$ K. Although we limit ourselves in the case of $H^{(1)} = H^{(2)}$, it should be noted that the thickness ratio, $H^{(2)}/H^{(1)}$, significantly affects on the swelling-induced bending state (Lucantonio et al., 2014). In the following part of this Section, we study the equilibrium shapes and stress distributions of the bilayer in the state of swelling-induced bending, focusing on the effects of the length-to-height (aspect) ratio, L/H, and the shear modulus ratio, $G^{(2)}/G^{(1)}$, which is related to the dimensionless crosslink density of gel, $n^{(2)}v_s$, through

$$\frac{G^{(2)}}{G^{(1)}} = \frac{n^{(2)}k_B T}{G^{(1)}} = \frac{(n^{(2)}v_s)\,k_B T}{G^{(1)}v_s} = 138 \cdot (n^{(2)}v_s).$$

3.1. Swelling-induced biaxial stress

Fig. 2 shows mechanical responses for gel layer under planar constraint in the kinematics from a dry state to the state of one-dimensional swelling as shown in Fig. 1(B). In Fig. 2(A), we plot the swelling ratio, equivalently the volume ratio $\left(J_0^{(2)} = V^{(2)}/V_0^{(2)} = \lambda_h^{(2)}\right)$, as a function of temperature T with three values of dimensionless crosslink density ($n^{(2)}v_s = 0.001, 0.005, 0.01$). We observe that the volume transition of the gel layer takes place at the LCST, $T \approx 305$ K, and exhibits the significant increase of its volume, equally swelling ratio $\lambda_h^{(2)}$, when the temperature decreases from above the LCST to below it. The inset in Fig. 2(A) shows the relation between the ratio of shear modulus of gel layer to that of elastomer layer, $G^{(2)}/G^{(1)}$, and the dimensionless crosslink density $n^{(2)}v_s$ of gel layer at $T = 300$ K. The values of $n^{(2)}v_s = (0.001, 0.005)$ imply the gel layer is softer than the elastomer layer according to their shear moduli, whereas the value of $n^{(2)}v_s = 0.01$ implies the gel layer is harder than the other. The lower values of $n^{(2)}v_s$ make the gel layer swell largely, and the swollen gel becomes softer than the dry state because the crosslink density $n^{(2)}$ is unchanged during swelling process. Fig. 2(B) also shows the swelling-induced biaxial stress $\sigma_0^{(2)}$ given by Eq. (10) which can induce the bending curvature of the bilayer. For the creation of self-folding structures in response to temperature, in the following results, we will focus on two equilibrium states across the LCST, at 310 K and 300 K, respectively.

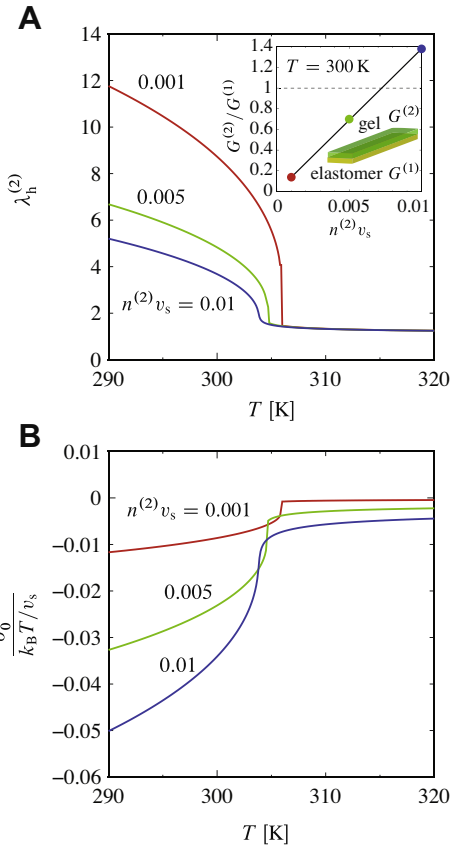

Fig. 2. Mechanical responses for gel layer under planar constraint. (A) Swelling ratio (stretch in the thickness direction) due to one-dimensional swelling. (B) Swelling-induced equi-biaxial compressive stresses.

3.2. Equilibrium shapes

In order to examine the equilibrium shapes of bilayer gels due to swelling responding to change in temperature, we first plot the bending curvature $\kappa^* = 1/r_i^{(1)}$ which is defined as the inverse of the radius of curvature at the inner surface of elastomer layer as a function of temperature T in Fig. 3. When the temperature decreases from above the LCST to below it, the curvature κ^* dramatically increases. The decrease of the dimensionless crosslink density $n^{(2)}v_s$ can induce the relatively large curvatures. The gel with lower value of $n^{(2)}v_s$ can take place large volume change due to swelling with its low elastic modulus. In order to capture the capability of our nonlinear model, we compare with the linear model calculated using Eq. (A.14), well-known as Timoshenko model (Timoshenko, 1925) based on elementary beam theory (see Appendix A). The linear model can provide the closed expression of the bending curvature due to the swelling-induced stresses given by Eq. (A.14), while cannot provide the stress distributions or the accurate geometry of the thickness. The significant quantitative difference between the nonlinear and linear models is observed at below the LCST. We suggest that the nonlinear model should be used accurately to predict the equilibrium shapes of bilayer gel involving large volume changes instead of the linear model. It is obvious that these results are valid for any values of the aspect ratio L/H of bilayer gel since the curvature does not depend on it in a pure bending problem. This fact is also supported by Eq. (A.12) in the linear model, which only depends on the ratios of the elastic modulus and thickness in a thin bilayer, (χ, δ).

Fig. 4 shows the self-equilibrium shapes at $T = 310$ K for various aspect ratios L/H and dimensionless crosslink densities $n^{(2)}v_s$. From Fig. 2(A), we see that the shapes below the LCST have almost no differences for three values of $n^{(2)}v_s = (0.01, 0.005,$

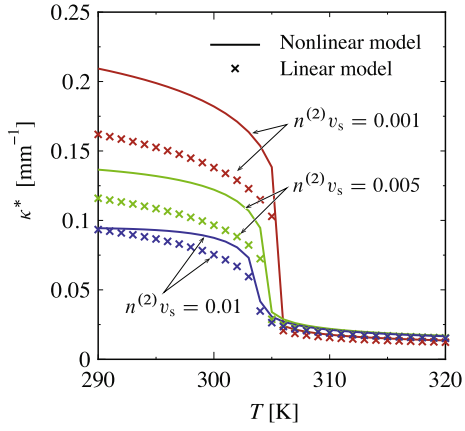

Fig. 3. Bending curvatures κ^* as a function of temperature T for bilayer gels with $n^{(2)}v_s = (0.1, 0.005, 0.01)$. The solid lines and the symbols correspond to the predictions from the nonlinear and linear model, respectively.

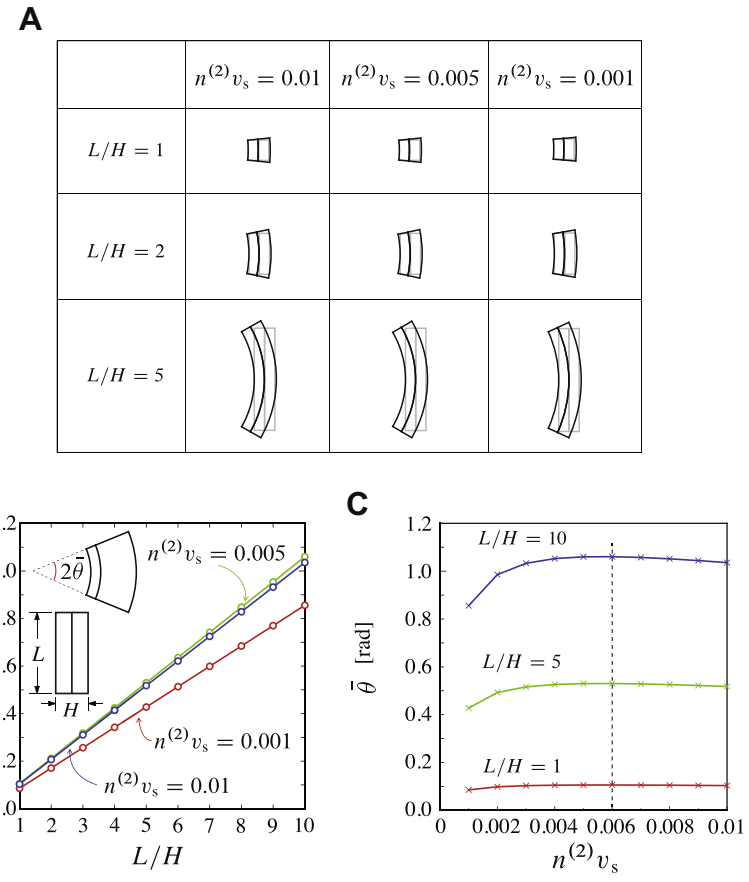

Fig. 4. Self-equilibrium shapes at $T = 310$ K, above the LCST. (A) Self-equilibrium shapes for various combinations of the normalized crosslink density $n^{(2)}v_s$ and aspect ratio L/H. (B) Bending semi-angle $\bar{\theta}$ as a function of the aspect ratio L/H for dry state with three normalized crosslink densities ($n^{(2)}v_s = 0.001, 0.005, 0.01$). (C) Bending semi-angle $\bar{\theta}$ as a function of the normalized crosslink density $n^{(2)}v_s$ with three aspect ratios ($L/H = 1, 5, 10$).

0.001), which correspond to the small swelling ratios at $T = 310$ K as indicated in Fig. 2(A). Fig. 4(B) indicates the linear response between the aspect ratio L/H and the bending semi-angle $\bar{\theta}$. This semi-angle $\bar{\theta}$ linearly increases with increasing the aspect ratio L/H. As mentioned above, the bending curvatures κ^* keep constant for varying the aspect ratios L/H in a pure bending problem. However, the bending semi-angles $\bar{\theta}$ are dependent on the aspect ratio L/H. That is, as the aspect ratio L/H increases, the bilayer gel forms a rolled shape with increasing bending semi-angle $\bar{\theta}$ while keeping the constant curvature κ^*. Fig. 4(C) shows that the normalized crosslink density $n^{(2)}v_s$ does not simply affect on the bending semi-angle $\bar{\theta}$. There exists the peak values of $\bar{\theta}$ at which $n^{(2)}v_s \sim 0.006$ for any values of L/H. This implies that to obtain a large bending actuation there may exist the optimized choices between the aspect ratio and the crosslink density. However, as for our specific settings at above the LCST, $T = 310$ K, the dependence of the bending semi-angle $\bar{\theta}$ on $n^{(2)}v_s$ is small enough to be negligible.

Fig. 5 shows the self-equilibrium shapes at $T = 300$ K for various aspect ratios and dimensionless crosslink densities $n^{(2)}v_s$. In Fig. 5(A) we observe that the gel layer is largely swollen and the self-folding structure is obviously formed depending on the normalized crosslink density $v^{(2)}v_s$ and the aspect ratio L/H. Fig. 5(B) shows the linear relation between the bending semi-angle $\bar{\theta}$ and the aspect ratio L/H. This is the same for the case of $T = 310$ K. When the bending semi-angle $\bar{\theta}$ becomes greater than the value of $\bar{\theta} = \pi$ at which both sides of bilayer gel are in self-contact, the equilibrium solution does not have the physical meaning due to the excess bending. We note that the stability analysis is required to determine the self-equilibrium states which can be physically realized. The inner surface of the bilayer can cause a localized buckling (Roccabianca et al., 2010) such as wrinkling, folding and creasing depending the ratio of shear modulus in the bilayer. However, as long as we deal with the self-equilibrium of bilayer gel subjected to pure bending in this paper, the bending moment in the bilayer at the self-equilibrium state is too small to pay attention to the stability until the threshold of excess bending, $\bar{\theta} \leqslant \pi$. This is behind the scope of the present investigation. In Fig. 5(C), we observe that the bending semi-angle $\bar{\theta}$ monotonically decreases with increasing the crosslink density $n^{(2)}v_s$. In contrast to Fig. 4(C), we found that the bending semi-angles $\bar{\theta}$ for $T = 300$ K has no peak values with respect to $n^{(2)}v_s$.

3.3. Stress distributions

In Fig. 6, we show the stress components $(\sigma_\theta^{(s)}, \sigma_r^{(s)})$ normalized by the shear modulus of elastomer layer $G^{(1)}$ for $T = 300$ K. The spatial variable $(r - r^{(1)})$ across the thickness of a bilayer is normalized by the total height of the bilayer in the current configuration, $h = h^{(1)} + h^{(2)}$. Since the stresses given by Eqs. (25) and (26) are only dependent on the r-direction, the stress profiles are independent of the aspect ratios L/H.

Fig. 6(A) shows the results for $n^{(2)}v_s = 0.01$, which correspond to the case that the shear modulus of gel layer $G^{(2)}$ is higher than that of the elastomer layer, $G^{(2)} > G^{(1)}$. On the other hand, Fig. 6(B) shows the results for $n^{(2)}v_s = 0.001$, which correspond to the case of $G^{(2)} < G^{(1)}$. From these figures, we can confirm the position of neutral axis at which the stress components being zero. This knowledge is valuable for designing the stretchable/flexible electronics where the active devices are placed on the neutral axis

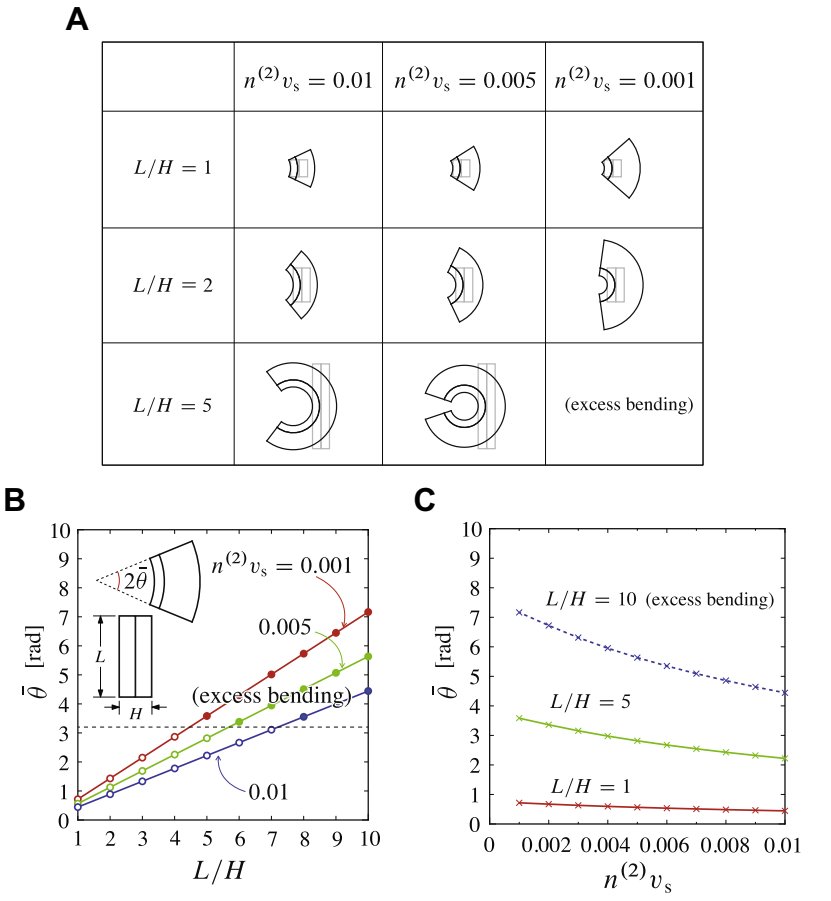

Fig. 5. Self-equilibrium shapes at $T = 300$ K, below the LCST. (A) Self-equilibrium shapes for various combinations of the normalized crosslink density $n^{(2)}v_s$ and aspect ratio L/H. (B) Bending semi-angle $\bar{\theta}$ as a function of the aspect ratio L/H for dry state with three normalized crosslink densities ($n^{(2)}v_s = 0.001, 0.005, 0.01$). (C) Bending semi-angle $\bar{\theta}$ as a function of the normalized crosslink density $n^{(2)}v_s$ with three aspect ratios ($L/H = 1, 5, 10$).

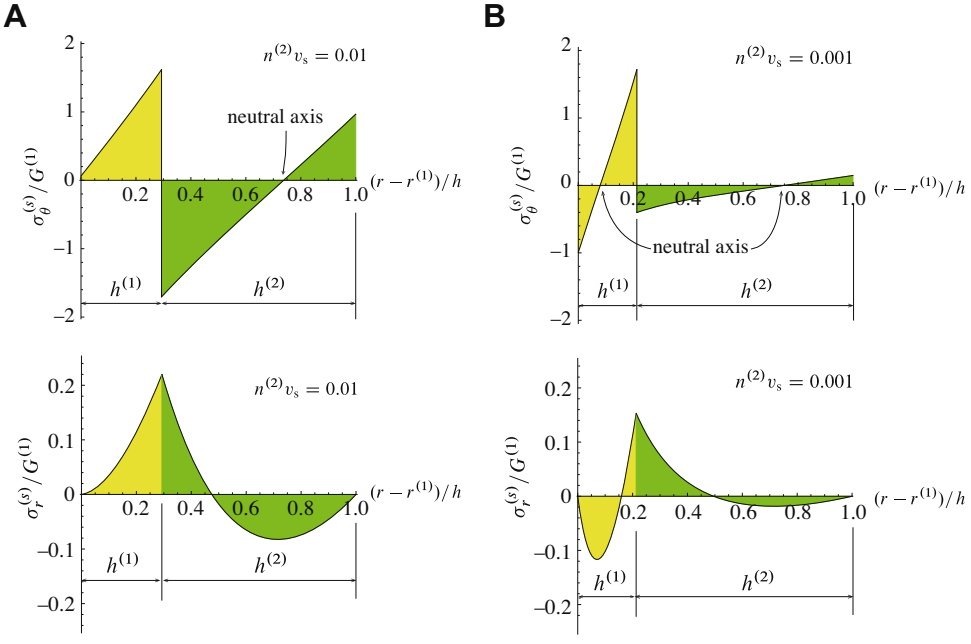

Fig. 6. Stress distributions for $T = 300$ K. Normalized stress components of (A) $n^{(2)}v_s = 0.01$ and (B) $n^{(2)}v_s = 0.001$.

to avoid failures during cyclic bending. In Fig. 6(B) for $n^{(2)}v_s = 0.001$, we notably observe there exist multiple neutral axes as a consequence of large strains in contrast to the case of $n^{(2)}v_s = 0.01$ where the single neutral axis exists. This fact that more than one neutral axis can occur has been known for bending of elastomeric multilayer with finite strain (Roccabianca et al.,

2010) and for bending of bilayer subjected to residual stresses with infinitesimal strain (Freund and Suresh, 2004).

The stress levels across the thickness of gel layer in Fig. 6(B) for $n^{(2)}v_s = 0.001$ are lower than those of the case for $n^{(2)}v_s = 0.01$. This is because the high swelling ratio makes the stress relax according to the volume expansion. Comparing the hoop stresses $\sigma_\theta^{(s)}/G^{(1)}$ in the case of $n^{(2)}v_s = 0.01$ and 0.001, the stress level within the gel layer is relatively low. The maximum stress is almost not changed because the elastomer layer deforms isochoricly without swelling. As is often the case with a layered structure, the interface maximizes the stress that may develop cracks during cyclic bending. To avoid stress concentration, we can use a structure having a large number of layers or a functionally graded structure since we expect that there is no obvious interface in such the structures. Actually, a composition-graded copolymer gels, prepared from hydrophobic and hydrophobic substrates, is available in the literature (Asoh et al., 2008). The procedure outlined in this paper can be extended to any number of layers and a graded layer with material properties varying in the thickness direction.

4. Conclusions

We investigated the temperature-responsive finite bending of bilayer gel under plane-strain condition. The bilayer gel was equivalently treated as specific bilayer consisting of a swellable gel layer and a non-swellable elastomer layer for brevity. The self-equilibrium shapes of the bilayer without any external forces were identified in terms of the bending curvatures κ^* and bending semi-angles $\bar{\theta}$, depending on the ratio of shear modulus $G^{(2)}/G^{(1)}$ and the aspect ratio L/H in the bilayer. We demonstrated that the bilayer model based on finite elasticity predicts larger curvatures compared with the linear model. The difference between both models was especially enhanced at below the LCST where the gel layer can induce large volume changes through the volume transition. This result suggests that the nonlinear model should be used accurately to predict the equilibrium shapes of bilayer gel involving large volume changes instead of the linear model.

We also showed that (i) the aspect ratio L/H influences on the semi-angle $\bar{\theta}$ while the curvature κ^* does not, and (ii) the normalized crosslink density $n^{(2)}v_s$ influences on both the bending semi-angle $\bar{\theta}$ and curvature κ^*. Furthermore, by quantifying the stress distributions at $T = 300$ K, we confirmed that multiple neutral axes can exist in the bilayer under certain conditions. Our analysis indicated that the folding shape of the bilayer can be controlled by tuning both the ratio of shear modulus $G^{(2)}/G^{(1)}$ and the aspect ratio L/H. The theoretical analysis in this paper could provide the basis for designing novel self-folding structures and offer opportunities for the development of programmable soft materials.

Appendix A. Linear model

In order to verify the capability of the nonlinear model presented in this paper, it is valuable to review the linear model well-known as Timoshenko model (Timoshenko, 1925) which can give the closed expression of the radius of bending curvature due to swelling-induced stresses. We use the coordinate system as shown in Fig. 1(B) by adapting to $O(\mathbf{e}_1, \mathbf{e}_2, \mathbf{e}_3) = O(x, y, z)$. Let us start by reviewing the Hooke's law:

$$\left.\begin{aligned} \varepsilon_x &= \tfrac{1}{E}[-\nu(\sigma_z + \sigma_x)], \\ \varepsilon_y &= \tfrac{1}{E}[\sigma_x - \nu\sigma_z] + \varepsilon_0, \\ \varepsilon_z &= \tfrac{1}{E}[\sigma_z - \nu(\sigma_x + \sigma_y)] + \varepsilon_0, \end{aligned}\right\} \tag{A.1}$$

where ε_0 is the residual strain due to lattice mismatch during film growth or due to thermal expansion. In this paper, we regard the residual strain as growth strain due to swelling. The strain in z-direction, ε_z, is independent of the position throughout the thickness of the bilayer, i.e., plane strain condition. The stress component in the thickness direction can be negligible $\sigma_x \approx 0$ by assuming that the thickness of bilayer gel is sufficiently thin. This assumption may no longer be valid for bilayer gel with large swelling. Instead, a finite bending theory should be required, which is developed in this paper. These assumptions yield

$$\left.\begin{aligned} \varepsilon_x &= -\tfrac{1}{E}\nu\sigma_z, \\ \varepsilon_y &= -\tfrac{1}{E}\nu\sigma_z + \varepsilon_0, \\ \varepsilon_z &= \tfrac{1}{E}(\sigma_z - \nu\sigma_y) + \varepsilon_0. \end{aligned}\right\} \tag{A.2}$$

From Eq. $(A.2)_3$,

$$\sigma_z = -E\varepsilon_0 + \nu\sigma_x. \tag{A.3}$$

Substituting into Eq. $(A.2)_2$ gives

$$\sigma_y = \bar{E}[\varepsilon_y - (1+\nu)\varepsilon_0], \tag{A.4}$$

where $\bar{E} = E/(1-\nu^2)$. The neutral axis defined in classical beam theory cannot be used to analyze the bending problem of bilayer subjected to residual stresses. Instead, the neutral axis can be obtained after the stress distribution in the system is solved (Hsueh, 2002). The bending strain in the y-direction ε_y is linear in x, namely,

$$\varepsilon_y = c + \frac{x - x_b}{R}, \tag{A.5}$$

where c is the constant strain and x_b defines the position of the plane where the bending strain is zero. Substituting Eq. (A.5) into Eq. (A.4),

$$\sigma_y = \sigma_b + \sigma_c, \tag{A.6}$$

where

$$\sigma_b = E'\left(\frac{x - x_b}{R}\right), \quad \sigma_c = E'[c - (1+\nu)\varepsilon_0]. \tag{A.7}$$

Assuming that no external forces are applied, the force balances due to uniform strain and bending strain and the bending moment with respect to the bending axis requires that

$$\left.\begin{aligned} &\textstyle\sum_{s=1}^{2}\sigma_c^{(s)}h^{(s)} = 0, \quad \sum_{s=1}^{2}\int_{x_i^{(s)}}^{x_i^{(s+1)}}\sigma_b^{(s)}\,\mathrm{d}x = 0, \\ &\textstyle\sum_{s=1}^{2}\int_{x_i^{(s)}}^{x_i^{(s+1)}}\sigma_y^{(s)}(x - x_b)\,\mathrm{d}x = 0, \end{aligned}\right\} \tag{A.8}$$

By solving the above three linear algebraic equations, we can obtain the three constants c, x_b, and $1/R$ as follows:

$$c = -\frac{(1+\nu^{(1)})\varepsilon_0^{(1)} + \eta\delta(1+\nu^{(2)})\varepsilon_0^{(2)}}{1+\eta\delta}, \tag{A.9}$$

$$x_b = h^{(1)}\left[\frac{1+\eta\delta(2+\delta)}{2(1+\eta\delta)}\right], \tag{A.10}$$

$$\frac{1}{R} = \frac{6\left[(1+\nu^{(2)})\varepsilon_0^{(2)} - (1+\nu^{(1)})\varepsilon_0^{(1)}\right]}{h^{(1)}} \times \left[\frac{(1-\eta\delta^2)^2 + 4\eta\delta(1+\delta)^2}{\eta\delta(1+\delta)}\right], \tag{A.11}$$

where $\eta = \bar{E}^{(2)}/\bar{E}^{(1)}$ and $\delta = h^{(2)}/h^{(1)}$. These expressions have been obtained by Timoshenko (1925) for a bimetal strip with different thickness and elastic modulus under plane stress condition and by Suo et al. (1999) for generalized plane strain condition. The more generalized expressions have provided by Nikishkov (2003) for a multilayer with different thickness and elastic modulus and Freund and Suresh (2004) for a compositionally graded layer.

In the physical system considered in this paper we have $E^{(2)}/3 = G^{(2)}$ and $\nu^{(1)} = \nu^{(2)} = 0.5$ for an isotropic, incompressible gel. Then, Eq. (A.11) reduces

$$\frac{1}{R} = \frac{h^{(1)}}{9\Delta\varepsilon_0}\left[\frac{\left(1-\eta\delta^2\right)^2 + 4\eta\delta(1+\delta)^2}{\eta\delta(1+\delta)}\right], \tag{A.12}$$

where $\Delta\varepsilon_0 = \varepsilon_0^{(2)} - \varepsilon_0^{(1)}$ is the misfit strain, which is calculated by Eq. (10):

$$\Delta\varepsilon_0 = \varepsilon_0^{(2)} - 0 = \frac{\sigma_0^{(2)}}{E^{(2)}} = \frac{\sigma_0^{(2)}}{6G^{(2)}} = \frac{1}{6n^{(2)}\upsilon_s}\frac{\sigma_0^{(2)}\upsilon_s}{k_BT}. \tag{A.13}$$

The coordinate system used here gives negative value of the radius of curvature R, the position of which is defined on the bending axis while the radius of curvature $r_i^{(1)}$ in the finite bending analysis is defined at the bottom surface of the elastomer layer ($s = 1$). For comparison between the linear and nonlinear models in the main text, we define the curvature at the bottom surface in the linear model to be the same as the nonlinear model:

$$\kappa_{\mathrm{lin}} \equiv \frac{1}{r_i^{(1)}} = \frac{1}{R - x_b}. \tag{A.14}$$

References

Afroze, F., Nies, E., Berghmans, H., 2000. Phase transitions in the system poly(N-isopropylacrylamide)/water and swelling behaviour of the corresponding networks. J. Mol. Struct. 554, 55–68.

Agrawal, A., Yun, T., Pesek, S.L., Chapman, W.G., Verduzco, R., 2014. Shape-responsive liquid crystal elastomer bilayers. Soft Matter 10, 1411.

Annabi, N., Tamayol, A., Uquillas, J.A., Akbari, M., Bertassoni, L.E., Cha, C., Camci-Unal, G., Dokmeci, M.R., 2013. 25th anniversary article: rational design and applications of hydrogels in regenerative medicine. Adv. Mater. 26, 85–124.

Asoh, T.a., Matsusaki, M., Kaneko, T., Akashi, M., 2008. fabrication of temperature-responsive bending hydrogels with a nanostructured gradient. Adv. Mater. 20, 2080–2083.

Azam, A., Laflin, K.E., Fernandes, R., Gracias, D.H., 2010. Self-folding micropatterned polymeric containers. Biomed. Microdevices 13, 51–58.

Bashir, R., 2004. BioMEMS: state-of-the-art in detection, opportunities and prospects. Adv. Drug Delivery Rev. 56, 1565–1586.

Byun, M., Santangelo, C.D., Hayward, R.C., 2013. Swelling-driven rolling and anisotropic expansion of striped gel sheets. Soft Matter 9, 8264.

Cai, S., Suo, Z., 2011. Mechanics and chemical thermodynamics of phase transition in temperature-sensitive hydrogels. J. Mech. Phys. Solids 59, 2259–2278.

Calvert, P., 2009. Hydrogels for soft machines. Adv. Mater. 21, 743–756.

Chester, S.A., Anand, L., 2010. A coupled theory of fluid permeation and large deformations for elastomeric materials. J. Mech. Phys. Solids 58, 1879–1906.

Chester, S.A., Anand, L., 2011. A thermo-mechanically coupled theory for fluid permeation in elastomeric materials: application to thermally responsive gels. J. Mech. Phys. Solids 59, 1978–2006.

Chester, S.A., Di Leo, C.V., Anand, L., 2015. A finite element implementation of a coupled diffusion–deformation theory for elastomeric gels. Int. J. Solids Struct. 52, 1–18.

Doi, M., 2009. Gel dynamics. J. Phys. Soc. Jpn. 78, 052001.

Dong, L., Agarwal, A.K., Beebe, D.J., Jiang, H., 2006. Adaptive liquid microlenses activated by stimuli-responsive hydrogels. Nature 442, 551–554.

Duda, F.P., Souza, A.C., Fried, E., 2010. A theory for species migration in a finitely strained solid with application to polymer network swelling. J. Mech. Phys. Solids 58, 515–529.

Flory, P.J., Rehner, J., 1943. Statistical mechanics of cross-linked polymer networks II. Swelling. J. Chem. Phys. 11, 521.

Freund, L.B., Suresh, S., 2004. Thin Film Materials. Stress, Defect Formation and Surface Evolution. Cambridge University Press, Cambridge.

Fukunaga, A., Urayama, K., Takigawa, T., DeSimone, A., Teresi, L., 2008. Dynamics of electro-opto-mechanical effects in swollen nematic elastomers. Macromolecules 41, 9389–9396.

Gracias, D.H., 2013. Stimuli responsive self-folding using thin polymer films. Curr. Opin. Chem. Eng. 2, 112–119.

Guan, J., He, H., Hansford, D.J., Lee, L.J., 2005. Self-folding of three-dimensional hydrogel microstructures. J. Phys. Chem. B 109, 23134–23137.

Hawkes, E., An, B., Benbernou, N.M., Tanaka, H., Kim, S., Demaine, E.D., Rus, D., Wood, R.J., 2010. Programmable matter by folding. Proc. Nat. Acad. Sci. 107, 12441–12445.

Hoare, T.R., Kohane, D.S., 2008. Hydrogels in drug delivery: progress and challenges. Polymer 49, 1993–2007.

Holmes, D.P., Roché, M., Sinha, T., Stone, H.A., 2011. Bending and twisting of soft materials by non-homogenous swelling. Soft Matter 7, 5188–5193.

Hong, W., Zhao, X., Zhao, X., Zhou, J., Suo, Z., 2008. A theory of coupled diffusion and large deformation in polymeric gels. J. Mech. Phys. Solids 56, 1779–1793.

Hsueh, C.H., 2002. Modeling of elastic deformation of multilayers due to residual stresses and external bending. J. Appl. Phys. 91, 9652.

Hu, Z., Zhang, X., Li, Y., 1995. Synthesis and application of modulated polymer gels. Science 269, 525–527.

Ionov, L., 2014. Hydrogel-based actuators: possibilities and limitations. Mater. Today.

Jamal, M., Zarafshar, A.M., Gracias, D.H., 2011. Differentially photo-crosslinked polymers enable self-assembling microfluidics. Nat. Commun. 2, 527.

Jeong, K.U., Jang, J.H., Kim, D.Y., Nah, C., Lee, J.H., Lee, M.H., Sun, H.J., Wang, C.L., Cheng, S.Z.D., Thomas, E.L., 2011. Three-dimensional actuators transformed from the programmed two-dimensional structures via bending, twisting and folding mechanisms. J. Mater. Chem. 21, 6824–6830.

Kang, M.K., Huang, R., 2010. A variational approach and finite element implementation for swelling of polymeric hydrogels under geometric constraints. J. Appl. Mech. 77, 061004.

Kelby, T.S., Wang, M., Huck, W.T.S., 2011. Controlled folding of 2D Au–polymer brush composites into 3D microstructures. Adv. Funct. Mater. 21, 652–657.

Kim, J., Hanna, J.A., Byun, M., Santangelo, C.D., Hayward, R.C., 2012. Designing responsive buckled surfaces by halftone gel lithography. Science 335, 1201–1205.

Kim, J., Hanna, J.A., Hayward, R.C., Santangelo, C.D., 2012. Thermally responsive rolling of thin gel strips with discrete variations in swelling. Soft Matter 8, 2375.

Klein, Y., Efrati, E., Sharon, E., 2007. Shaping of elastic sheets by prescription of non-euclidean metrics. Science 315, 1116–1120.

Kumar, K., Nandan, B., Luchnikov, V., Simon, F., Vyalikh, A., Scheler, U., Stamm, M., 2009. A novel approach for the fabrication of silica and silica/metal hybrid microtubes. Chem. Mater. 21, 4282–4287.

Lucantonio, A., Nardinocchi, P., Pezzulla, M., 2014. Swelling-induced and controlled curving in layered gel beams. Proc. R. Soc. A-Math. Phys. 470, 20140467–20140477.

Lucantonio, A., Nardinocchi, P., Teresi, L., 2013. Transient analysis of swelling-induced large deformations in polymer gels. J. Mech. Phys. Solids. 61, 205–218.

Luchnikov, V., Sydorenko, O., Stamm, M., 2005. Self-rolled polymer and composite polymer/metal micro- and nanotubes with patterned inner walls. Adv. Mater. 17, 1177–1182.

Majidi, C., 2014. Soft robotics: a perspective-current trends and prospects for the future. Soft Rob. 1, 5–11.

Nikishkov, G.P., 2003. Curvature estimation for multilayer hinged structures with initial strains. J. Appl. Phys. 94, 5333.

Osada, Y., Gong, J.P., 1998. Soft and wet materials: polymer gels. Adv. Mater. 10, 827–837.

Peppas, N.A., Hilt, J.Z., Khademhosseini, A., Langer, R., 2006. Hydrogels in biology and medicine: from molecular principles to bionanotechnology. Adv. Mater. 18, 1345–1360.

Randall, C.L., Gultepe, E., Gracias, D.H., 2012. Self-folding devices and materials for biomedical applications. Trends Biotechnol. 30, 138–146.

Richter, A., Howitz, S., Kuckling, D., Arndt, K.F., 2004. Influence of volume phase transition phenomena on the behavior of hydrogel-based valves. Sens. Actuators B: Chem. 99, 451–458.

Rivlin, R.S., 1949. Large elastic deformations of isotropic materials. V. The problem of flexure. Proc. R. Soc. A-Math. Phys. 195, 463–473.

Roccabianca, S., Gei, M., Bigoni, D., 2010. Plane strain bifurcations of elastic layered structures subject to finite bending: theory versus experiments. IMA J. Appl. Math. 75, 525–548.

Schild, H.G., 1992. Poly(N-isopropylacrylamide): experiment, theory and application. Prog. Polym. Sci. 17, 163–249.

Sharon, E., Efrati, E., 2010. The mechanics of non-euclidean plates. Soft Matter 6, 5693.

Smela, E., Inganas, O., Lundstrom, I., 1995. Controlled folding of micrometer-size structures. Science 268, 1735–1738.

Stuart, M.A.C., Huck, W.T.S., Genzer, J., Müller, M., Ober, C., Stamm, M., Sukhorukov, G.B., Szleifer, I., Tsukruk, V.V., Urban, M., Winnik, F., Zauscher, S., Luzinov, I., Minko, S., 2010. Emerging applications of stimuli-responsive polymer materials. Nat. Mater. 9, 101–113.

Studart, A.R., Erb, R.M., 2014. Bioinspired materials that self-shape through programmed microstructures. Soft Matter 10, 1284–1294.

Suo, Z., Ma, E.Y., Gleskova, H., Wagner, S., 1999. Mechanics of rollable and foldable film-on-foil electronics. Appl. Phys. Lett. 74, 1177.

Swann, J.M., Ryan, A.J., 2009. Chemical actuation in responsive hydrogels. Polym. Int. 58, 285–289.

Therien-Aubin, H., Wu, Z.L., Nie, Z., Kumacheva, E., 2013. Multiple shape transformations of composite hydrogel sheets. J. Am. Chem. Soc. 135, 4834–4839.

Timoshenko, S., 1925. Analysis of bi-metal thermostats. J. Opt. Soc. Am. 11, 233.

Topham, P.D., Howse, J.R., Crook, C.J., Armes, S.P., Jones, R.A.L., Ryan, A.J., 2007. Antagonistic triblock polymer gels powered by pH oscillations. Macromolecules 40, 4393–4395.

Wu, Z.L., Moshe, M., Greener, J., Therien-Aubin, H., Nie, Z., Sharon, E., Kumacheva, E., 2013. Three-dimensional shape transformations of hydrogel sheets induced by small-scale modulation of internal stresses. Nat. Commun. 4, 1586.

Yu, Y., Nakano, M., Ikeda, T., 2003. Photomechanics: directed bending of a polymer film by light. Nature 425, 145–155.

Zhang, J., Wu, J., Sun, J., Zhou, Q., 2012. Temperature-sensitive bending of bigel strip bonded by macroscopic molecular recognition. Soft Matter 8, 5750–5752.